Sustainable

Engineering and Technological Sciences

https://sets.zenithacademic.co.uk/index.php/sets/index

Sustainable Engineering and Technological Sciences, 01(01), 2025, pp. 71-89
DOI: https://doi.org/10.70516/7a9e2y30

ISSN 3049-7787 (Print)
ISSN 3049-7795 (Online)

Overcoming Boundary-Layer Separation with Distributed Propulsion

Adam Suppes [1,a*], Galen Suppes [2,b], Harith H. Al-Moameri [3,c]

[1] Suppes Engineering Technologies, 5400 S Hyde Park Blvd Apt D7, Chicago, IL 60615-5852.
[2] HS-Drone LLC, 710 Lexington Ave., Charlottesville, VA 22902.
[3] Materials Engineering Department, Faculty of Engineering, Mustansiriyah University, Baghdad 35010, Iraq.

[a] asuppes@seas.upenn.edu (https://orcid.org/0009-0007-5719-7907)
[b] Corresponding author's email: suppesg@hs-drone.com. (https://orcid.org/0000-0002-3076-4955)
[c] almoamerih@uomustansiriyah.edu.iq. (https://orcid.org/0000-0001-5985-0235)

Article info
Received 24 December 2024
Revised 28 December 2024
Accepted 29 December. 2024
Available online 1 Jan. 2025

Keywords: *Aircraft; Trucks; Efficiency; Lift; Drag; Rolling Losses; Mechanical Resistance; Distributed Propulsion.*

Abstract. Strategically located propulsors are able to create constructive interference on aircraft; increasing lift, lift-drag ratios (L/D), and resilience to boundary layer separation. Computational fluid dynamic (CFD) studies teach toward an optimal configuration with a near-zero upper-surface pitch in front of a trailing section propulsor followed by a trailing taper with 20° to 45° surface pitch from the propulsor to a trailing edge near the bottom of the lifting body ("Lift Span Tech"). Applications benefiting from Lift Span Tech range from box trucks to high-speed intercontinental transit. With initial propulsor power mitigating boundary layer separation, Lift Span Tech provides a high gain:loss, where the gain is in reduced drag and loss is reduced thrust from the propulsor. Performance may be augmented with ground effect further improving L/D efficiency. This study evaluates the sensitivity of performance to different CFD turbulence models and trailing taper pitches. While today's commercial approaches can reduce truck drag by about 34% with no impact on wheel friction, new Lift Span Tech is able to reduce drag by up to 84% and wheel friction by up to 90%. The technology enables designs to allow direct solar power to fully replace liquid fuels in a wide range of vehicles.

1. Introduction

Propulsor intakes create lower pressures and discharges create higher pressures; these propulsor-generated pressures are valuable degrees of freedom to optimize lift-drag ratios of lifting bodies. The same configurations are able to overcome boundary-layer separation that is otherwise detrimental to performance caused by sudden changes in surface pitches at upper-surface trailing-sections and propulsors.

CFD simulations enable rapid progress on understanding effective-use configurations referred to as Lift Span Tech. Lift Span Tech is able to overcome induced drag which has stifled the use of ground effect machines (GEM) to further increase L/D efficiency. A few of the applications are solar-powered cars, box trucks, mass transit, and inter-continental transit.

While the ability to qualitatively and quantitatively relate pressure profiles to L/D is a standard outcome of CFD simulations, quick metrics to quantify [incremental gain in reduced drag]:[incremental loss in propulsion] are not yet standard analyses. Lost work analyses are able to supplement preliminary CFD results where extended CFD studies and prototypes a quite extensive in scope.

This paper uses CFD analysis to evaluate representative lifting bodies which are supplemented by lost work analyses. Results include 3D CFD results on

representative digital prototype GEM including applications to box trucks.

2. Background

A common source of lost lift pressures from airfoils occurs with boundary layer separation. Boundary layer separation occurs when the laminar flow parallel to the airfoil splits away and develops eddy currents [1, 2]. These eddy currents have higher pressure than the laminar flow preceding it due to high turbulence. The turbulent flow created by boundary layer separation also induces a large amount of noise pollution, also indicative of energy loss [3, 4]. Most commonly, boundary layer separation occurs at low Reynolds number and high angle of attack; from a strong curvature of the airfoil perpendicular to the direction of flow.

Mitigation and prevention of boundary layer separation is an active area of research to improve airfoil efficiency and stability. Rodriguez et. Al. and others have investigated using surface structures, such as actuators and biologically inspired structures such as shark fins, to disrupt the formation of boundary layer separation [5-8]. These studies have shown that boundary layer separation may be prevented with these structures, however, it does not generally increase airfoil efficiency [9]. Wang and Lai investigated the impact of boundary layer suction on prevention of boundary layer separation and noise reduction [10, 11]. Expanding on previous research focusing on one region of boundary layer separation, they investigated both a suction boundary layer prior to boundary layer separation and a section region prior to general boundary layer separation locations. They determined that while individually a single section produces mixed results: front end boundary layer separation delays but does not prevent boundary layer separation while rear end boundary layer separation on changes the flow from the suction area to the trailing edge. However, in combination, the two regions prevent the formation of boundary layer separation, increasing the lift coefficient by 12.53% and decreasing the drag coefficient by 27.93% [11].

Due to the rapid reduction of L/D efficiency with the onset of boundary layer separation, it is possible for strategically designed propulsion to provide much greater "effective thrust" than from the mere momentum generated in the air by the propulsor. The placement of propulsors has been an active topic of investigation, including incorporation into tails and upper surfaces, particularly with synergistic activity of distributed propulsion [12-26]. Figure 1 illustrates how the strategic placement of a propulsor leads to an operating point at lower power (i.e., force times velocity) and correspondingly higher effective efficiency [27].

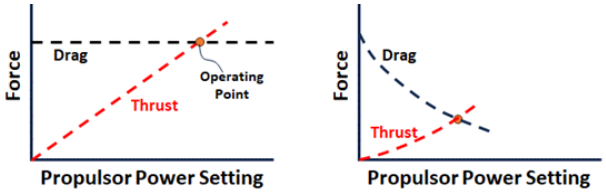

Figure 1. Illustration of how strategic placement of propulsion can reduce thrust needed for propulsor including a base case (left) with no interference from a propulsor and a case with constructive interference (right).

Constructive interferences can lead to more-efficient operating points including: reduced induced drag (including prevention of boundary-layer separation phenomena), increased induced thrust, and enhanced ground-effect lift from a lower cavity of a GEM. A more expansive illustration of Figure 1 is provided by Figure 2 [28].

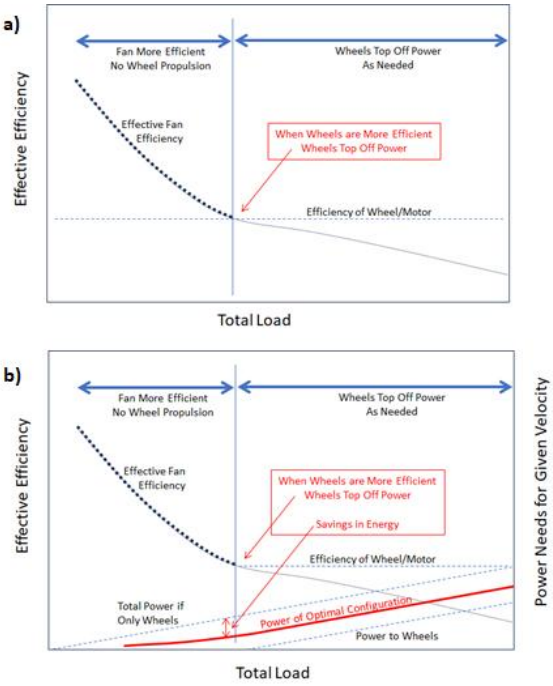

Figure 2. Illustration of optimal operation for propulsor that reduces drag as power increases: a) at lower total loads, the fan is more efficient than wheels and b) when wheel propulsion tops off fan propulsion at higher loads a savings in energy is achieved [28].

One application of the Figure 2 efficiency balances is to elucidate how Lift Span Tech can reduce power for a box

truck through optimal use of Lift Span Tech on the box with wheel-based thrust augmenting the air-based thrust in an overall optimal configuration. The resulting box truck may resemble a GEM with lift provided by a lower surface cavity where Lift Span Tech propulsion may be augmented by any of a variety of propulsion means, including wheels, linear motors, and other air-based propulsion. A representative CFD mesh for Lift Span Tech is provided by Figure 3.

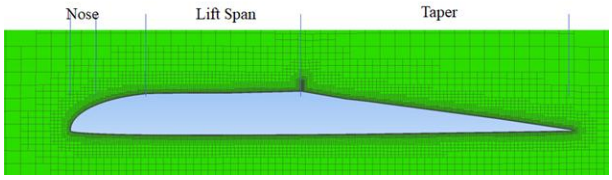

Figure 3. CFD mesh of a lifting body fuselage with Lift Span Tech. The upper-surface propulsor is between the Lift Span and the trailing Taper.

By overcoming boundary layer separation, Lift Span Tech is able to truncate the chord length of lifting bodies; whereby, the L/D efficiency of GEM have traditionally been corelated with [ground clearance]:[lifting body chord} an alternative correlation of L/D efficiency with [ground clearance]:[lifting body height] emerges [29-37]. This alternative correlation allows fuselages to be used as lifting bodies in GEM without the need for extensive chord lengths.

As compared to conventional upper-surface trailing-section propulsors, Lift Span Tech has: a) a lower-surface pitch area in front of propulsor and b) a significant change in surface pitch aft the propulsor versus fore the propulsor. Previous works identified advantages of: a) increasing lift by reducing induced drag and b) allowing the length of a ground-effect machine to be reduced with related practical advantages.

In a benchmark Smith patent GEM design, the commercial potential was limited by issues with reduced drag and extensive chord lengths [38]. Figure 4 compares the Smith airfoil to a Lift Span Tech airfoil. Figure 4 identifies a propulsor at the same locations on both airfoils. GB1347352 (Smith GEM) identified a forward crossover propulsor which can reduce the speed needed for air-based propulsion but did not provide innovations to overcome issues with induced drag or long chord lengths.

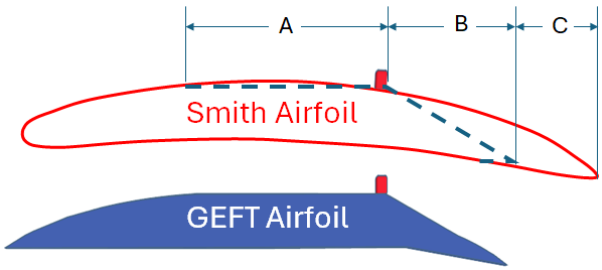

Figure 4. Comparison of GB1347352 to Ground Effect Flight Transit (GEFT) centerline wing sections with indication of GEFT propulsor.

Figure 5 compares a preferred vehicle design, referred to as ground effect flight transit (GEFT), to the Smith GEM. The Smith GEM uses a lower-surface perimeter that extends lower than its lower-surface cavity. In contrast, GEFT uses cavity side fences as control surfaces and a more-open cavity front. When in ground-effect flight, higher L/D efficiency is achieved when the side fences have a near-constant clearance with the ground.

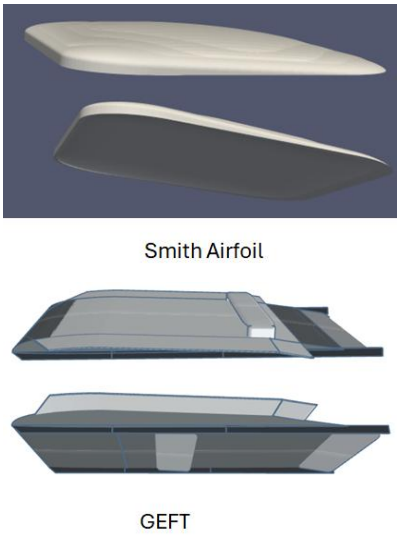

Figure 5. Comparison of GB1347352 STL model (Smith GEM) to GEFT. The preferred propulsion for the Smith Airfoil is a crossover propulsor (not shown) while the preferred propulsion for GEFT is an upper-surface trailing-section propulsor in a Lift Span Tech configuration.

Contrary to common theories of aerodynamic lift that associate aerodynamic lift with conversions between air's relative velocity and pressure, the GEFT design is based on six principles based on fundamental physics and their derivatives [39, 40]. Energy balances dictate that velocity can transform to pressure and visa-versa; however, the velocity-pressure transformation is: a) one of multiple

transformation that generate and expand aerodynamic lift pressures and b) is incomplete in identifying the causes of generation and loss of lift pressures.

The six principles identify how pressure both extends its influence and dissipates at the speed of sound. The most-efficient ground effect flight is achieved when both the ground and fences block the dissipation of lift forces from the lower cavity. Conversions between velocity and pressure are implicit within the energy balance in GEM design; however, the respective conversions lack causality which is ineffective towards extrapolation, innovation, and improved designs. The six following principles enable extrapolation, innovation, and improved designs.

Principle 1. Impacting air flows create higher surface pressures.

Principle 2. Diverging air flows create lower surface pressures.

Principle 3. Air flowing from higher to lower pressures at the speed of sound extends lift pressures along streamlines, dissipates lift pressures across streamlines, and interacts with air flow to turn streamlines.

Principle 4. The L/D of a section of an airplane surface is approximately equal to 57° divided by the pitch of the surface in degrees for lower surfaces and -57° divided by the pitch for upper surfaces. The pitch angle is relative to horizontal with the nose up as positive.

Principle 5. Surfaces can be used to block loss of lift pressures leading to increased L/D. Example surfaces are winglets on wing tips and fences under lifting bodies.

Principle 6. For a ground-effect aircraft with a properly-designed lower fenced cavity, 3D CFD estimates of cavity lift pressures are able to approach 2D estimates, enabling 2D airfoil simulations to accurately predict actual performances and trends in many applications.

Sister papers provide further details of the six principles' validation with both continuum and discrete mechanics, as well as how lost work analysis can teach toward optimal designs. The Figure 6 CFD results are particularly insightful per the lost work analysis and the fundamental phenomena supporting Figure 2 [39, 40, 27].

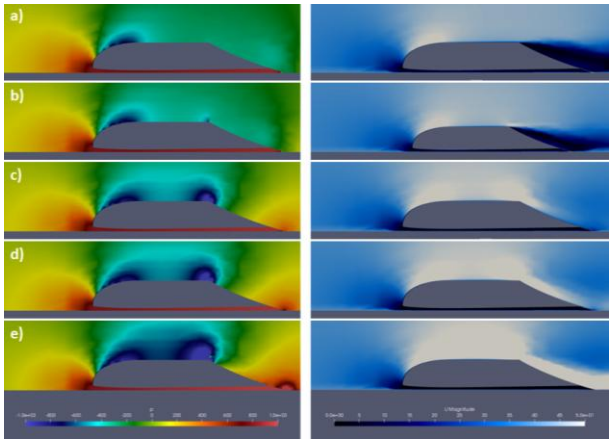

Figure 6. Pressure and velocity profiles of high thickness ratio GEFT wing sections. Pressure (P) is in m^2/s^2 and velocity (U) is in m/s.

Lower propulsor settings with lift span tech (6a, 6b) continue to have turbulence with lower pressures above the trailing taper leading to: lower pressures, induced drag, and excess energy exiting as velocity gradients between exiting streamlines. At higher propulsor settings (6d, 6e), jet wash is exhibited between exiting streamlines with similar loss of available energy. An optimal setting is in the absence of significant velocity gradients between exiting streamlines with minimal available energy exiting in streamlines. This optimal setting is consistent with the average pressure above the trailing taper approaching near-free-stream pressure.

In summary: a) the ground blocks loss of available energy downward, b) fences block loss of available energy spanwise, and c) optimal application of Lift Span Tech reduces loss of available energy in air exiting the trailing section of a control volume containing the lifting body. While air-based propulsion often emphasizes the creation of momentum in the air as the source of thrust; when designing propulsors for constructive interference with a lifting body surface, the creation of pressure gradients—which expand at the speed of sound—tends to be of equally-high importance to use of the lifting body to generate induced thrust and to minimize available energy in exiting streamlines.

This paper provides additional data to support previous works, including: a) the impact of different turbulence models to provide insight into the impact of CFD simulation accuracy on the results, b) the impact of different pitch angles of Lift Span Tech's trailing taper, and c) preliminary CFD results on a box truck to reduce drag using Lift Span Tech. Previous work identified how ground-effect flight bridges the gap between flight and rail

transit; this work identifies how the optimal designs for planes, trains, and automobiles may incorporate lift span and ground effect technologies [41-48]. The bridging of the gaps includes applications for trucks and boats.

3. Experimental Methods

OpenFOAM CFD software was used to simulate digital prototypes from prepared STL files. Methods were matched to maintain fidelity and methods analogous to those within the field [49-52, 29]. Two-dimensional (2D) simulations were used to identify trends in performance while 3D simulations were performed on the final prototypes and key designs. Unless otherwise reported, the scale chords of the STLs were 1 m, the fluid was air at 1 atm pressure, and the free stream velocity was 40 m/s. Pressure profiles are symmetrically presented with blue as low pressures, red as high pressures, and passing through green at 0 gauge pressure. Computer aided design (CAD) was used to create STL files for the Smith Airfoil and GEFT by combining common geometries.

For ground effect simulations, the ground was simulated as a lower boundary condition with a velocity equal to the free stream air. Velocity profiles are from the reference frame of the airfoil/digital prototype. Unless otherwise identified, the propulsion sources were rectangular with a height of 2 cm and thickness of 2 mm. Free steam flow boundaries were simulated at a minimum of 10 chord lengths from the vehicle in free stream directions.

Both 2D and 3D CFD simulations were performed. 2D simulations are referred to as being performed on airfoils or wing sections. Some 2D simulations were performed with SimFlow software. 3D simulations are referred to as being performed on digital prototypes or GEM.

4. Results

Early work leading to Lift Span Tech in free flight is summarized by Table 1 and Figure 7 [47, 53]. The free flight L/D performances are not as high as the ground effect performances, but several trends are consistent:

- The sudden increase in the upper-surface's pitch at the onset of the trailing taper leads to boundary layer separation at propulsor settings of zero.
- The propulsor is able to overcome boundary layer separation; a sudden increase in L/D is observed as boundary layer separation is mitigated.
- The onset of better L/D efficiencies correlates with the appearance of a trailing-edge taper in a design with a robust leading-edge taper.
- Induced thrust at the frontal section increases with increasing propulsor power.

For GEM wing sections, higher L/D efficiencies are attained due to the ground blocking the downward loss of lift pressures. The Figure 7 data illustrates how optimal Lift Span Tech uses a morphing surface with lower pitches at the trailing taper at lower propulsor settings [53].

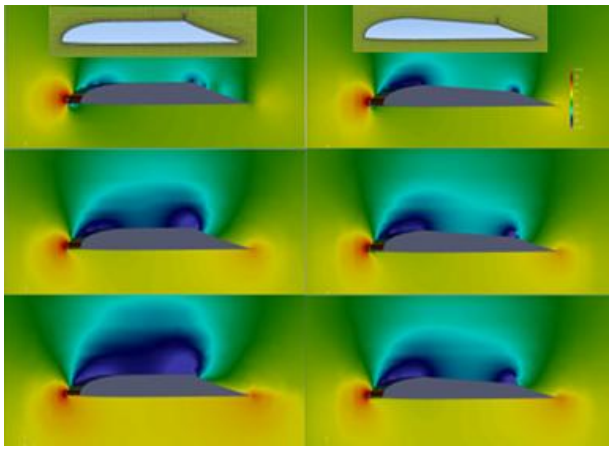

Figure. 7. Pressure profiles of wing sections and performance data illustrating Lift Span Technology. S designates the Source/Propulsor setting.

Table 1. Preliminary Lift Span Tech data.

		-1° Lift Span			4° Lift Span		
FS (m/s)	**S (m4/s2)**	**cl**	**cd**	**L/D**	**cl**	**cd**	**L/D**
40	0	0.251	0.0338	7.4	0.339	0.0219	15.5
40	20	0.527	0.0157	33.5	0.477	0.0186	25.6
40	40	0.607	0.0092	65.8	0.548	0.0163	33.6

The optimal morphing surface configurations can be attained through result's driven optimization [29, 34, 36, 54, 55]. Figure 8 illustrates several airfoils evaluated to identify trends of the trailing section taper on performance. Figure 9 summarizes the pressure profiles and select velocity profiles.

Wing section 8a at a trailing taper at 70° failed to develop a strong trailing edge stagnation point and did not perform well. Wing section 8b was equipped with a source with an entrance at -45º pitch and exit flow adjusted with horizontal ("x") and vertical ("y") components as summarized by Table 2.

As summarized by Table 2 for profiles 9b and 9c, performance was poor with only horizontal flow through the propulsor. Only when the flow through the source had equal vertical and horizontal components was reasonable

performance achieved. However, the L/D efficiencies did not achieve the higher L/D of the Figure 6 airfoil.

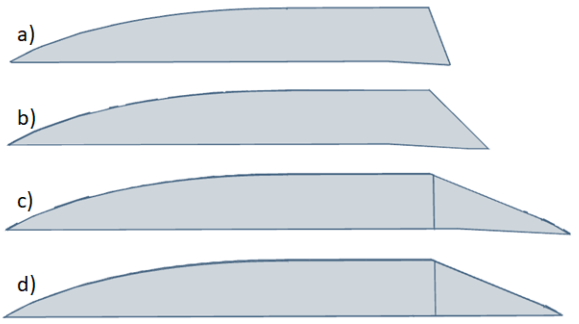

Figure 8. Images of airfoils for study of trailing taper with horizontal upper and lower mid-chord surfaces and trailing taper surface pitches of a) 70°, b) 45°, c) 25° and d) 25° without a flap.

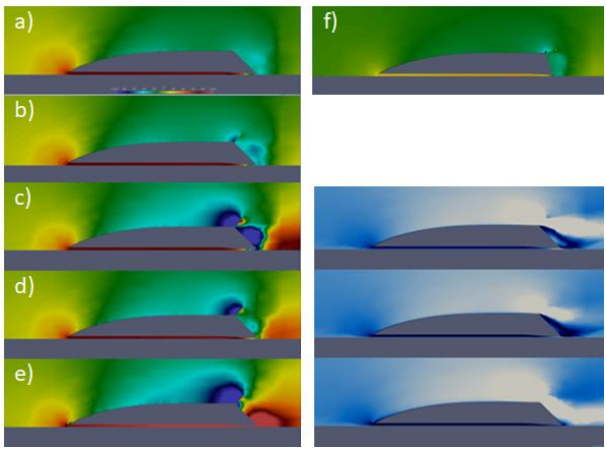

Figure 9. Pressure profiles of wing sections with 45° taper (a-e) with velocity profiles on right in blue scale (0 to 50 m/s). Pressure image f is for a 70° trailing taper. Performances are in Table 2. The pressure scale is ±1000 m^2/s^2 and velocity scale is 0 -50 m/s.

Table 2. L/D efficiencies of wing sections at free stream velocity of 40 m/s. Data for Figures 6 and 9.

Figure	S_x (m4/s2)	S_y (m4/s2)	L/D
9a	0		18.1
9b	2.5		15.9
9c	20		9.1
9d	5	-5	26.0
9e	10	-10	-64.8
9f	20		9.1
6a	0		20
6b	1		21
6c	2.5		42
6d	5		53
6e	20		533

Figure 10 compares the performance of the 8c airfoil with and without a trailing flap with Table 3 summarizing the L/D efficiencies. The data indicates that a trailing-edge stagnation point can function as a flap when it is sufficiently robust; in this example that is for propulsor settings above about 2 m^4/s^2. Additional simulations identify that the trailing edge stagnation point is influenced by the proximity of the trailing edge of the airfoil to the ground. Air flows of different vectors create higher pressures when they collide, but collision with a solid surface is more efficient in generating higher-pressure regions.

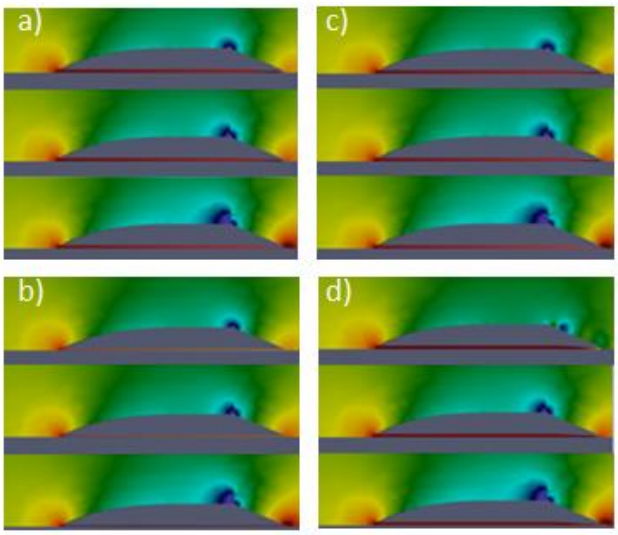

Figure 10. Pressure profiles of 8c airfoil with: a) with k-ω SST turbulence model, b) with k-ω SST turbulence model and no flap, c) Spalart Allmaras turbulence model, and d) laminar flow model. Source settings are 0, 1, and 5 $m4/s_2$.

The absence of a flap leads to lower pressure drag as identified by Table 3. It is a reasonable deduction based on air impacting the flap with the creation of higher pressures.

A comparison of turbulence models is provided by Figure 10 and Table 3. The primary anomaly with the pressure profiles is for laminar flow. At zero propulsor power, an instability in the CFD solution manifests at the trailing taper. The laminar flow model fails in convergence due to the geometry and flight conditions' inconsistency with laminar flow.

Within the interpretation made by this study, the two turbulence models are in agreement on L/D efficiency. These two models are consistent with the laminar flow model at propulsor settings of 1 and 5 m^4/s^2.

Table 3. Summary of turbulence model comparison and impact of flap for wing sections of Figure 10. The drag coefficients are not normalized to the wing section area.

	S	L/D	Cd		
	(m4/s2)	L/D	Total	Pressure	Viscous
a) k-w SST	0	56	0.00240	0.00197	0.00043
	1	66	0.00210	0.00165	0.00044
	5	131	0.00115	0.00067	0.00049
b) No Flap	0	37	0.00210	0.00149	0.00061
	1	49	0.00179	0.00119	0.00060
	5	165	0.00077	0.00017	0.00060
c) Spalart-Allmaras	0	51	0.00266	0.00210	0.00056
	1	59	0.00236	0.00178	0.00058
	5	107	0.00143	0.00079	0.00064
d) Laminar	0	28	0.00423	0.00407	0.00016
	1	77	0.00171	0.00154	0.00017
	5	175	0.00081	0.00066	0.00015

Turbulence creates a higher viscous drag than laminar flow, which is expressed in the data of Table 3. A conclusion is that turbulence exists at some level, most likely at the trailing flap, but the detrimental impact of boundary layer separation on performance does not manifest.

The primary factor leading to high L/D efficiency with increasing propulsor power is the reduction in induced drag behind the trailing Taper. Induced thrust on upper-surface forward sections also decreased the total drag based on the magnitudes of the lower pressure region forward of the propulsor.

CFD studies toward applying GEFT technology to a box truck are summarized by STL models in Figure 11 and by pressure and velocity profiles in Figure 12. The studies include a progression of adding a forward deflector in an aerodynamic nose, a trailing taper, and a lower surface cavity, followed by a GEFT design for comparison and modified GEFT for wheeled ground transit. CFD profiles are summarized by Figure 12 with performances summarized by Table 4.

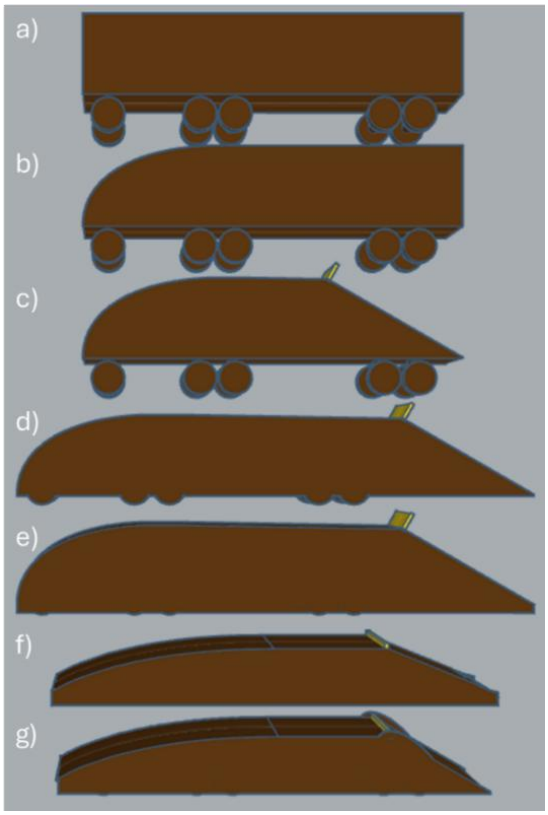

Figure 11. STL images of box truck configurations. From top to bottom: a) Box configuration, b) Aerodynamic nose, c) Trailing 30-degree taper and Sourcebox, d) Extended trailer with 30-degree taper, Sourcebox, and 0.1 clearance on body, and e) fence of 0.02 clearance added to d with i: no flap and ii: trailing flap at 60% of fence extension, f) GEFT comparison design, and g) GEFT with trailing taper fence and wheels.

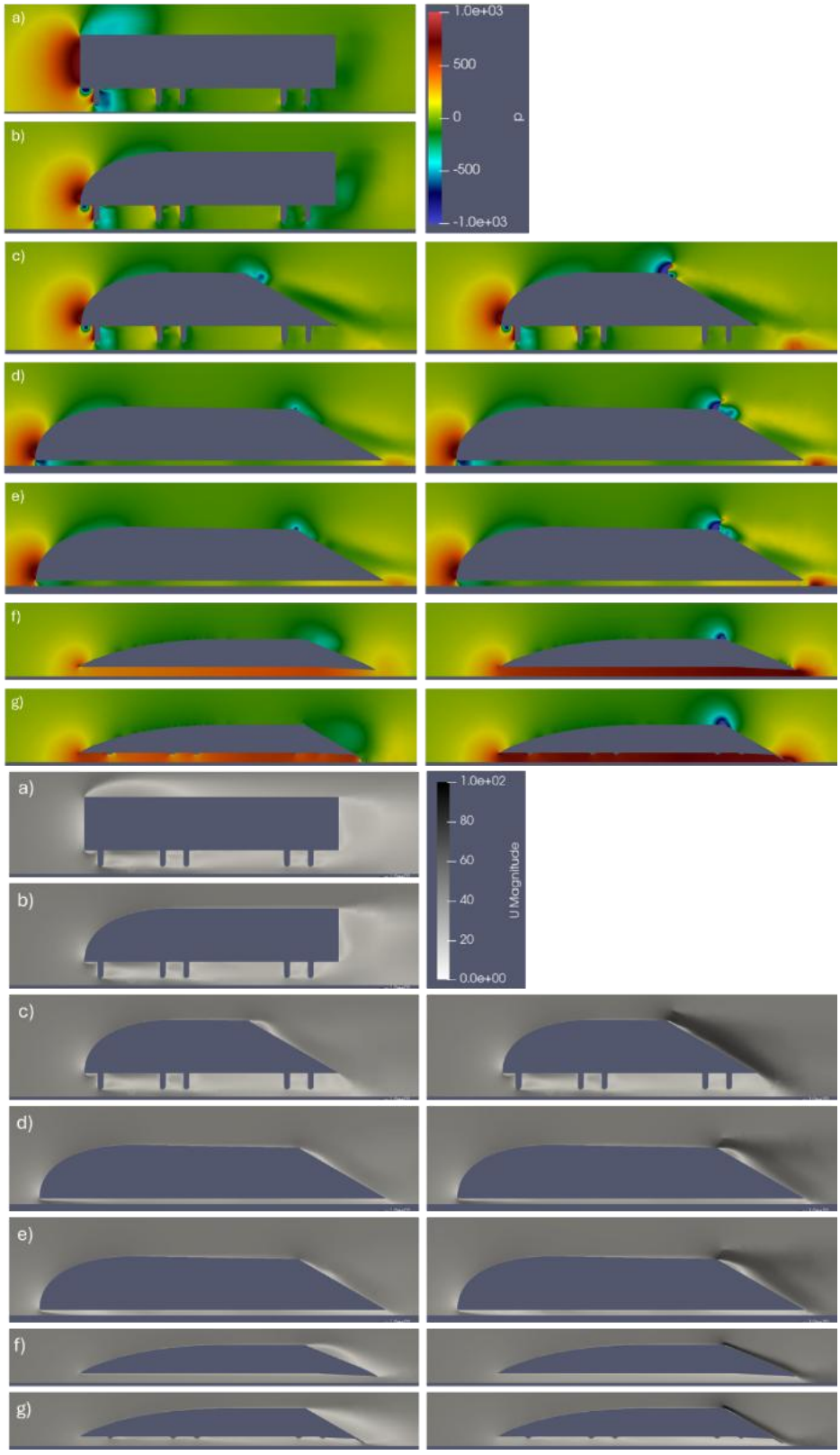

Figure 12. Pressure and velocity profiles for box trucks and GEFTs of Figure 11. Left column: No active source. Right column: 5 Source at 30 degrees aligned with tapers (only for trailers with tapers: c-e); 2.5 Source horizontal flow for GEFT (f ang g). (a)-(c) are 0.84m in length, (d) and (e) are 1.17m in length, (f) is 1m in length, and (g) is 0.97m in length. Travel is 40m/s. Source is 4mm by 0.4mm for box trucks and 1mm by 0.5mm for GEFT.

Table 4. Specifications and coefficient of drag data for box truck pressure profiles of Figure 12.

Trailer	Source Power	Source Angle	Cd	Cd viscous	Cd pressure	L/D	Aspect Ratio
a) Trailer1_block	0	0	0.2636	0.00838	0.2518	0.2636	0.16
b) Trailer2_nose	0	0	0.1878	0.01705	0.1678	0.1878	0.16
c) Trailer3_Taper	0	0	0.1860	0.01465	0.1684	0.1860	0.16
Trailer3_Taper	10	30	0.1843	0.01973	0.1643	0.1843	0.16
Trailer3_Taper	5	30	0.1878	0.01740	0.1669	0.1878	0.16
Trailer3_Taper	10	0	0.2171	0.01936	0.1973	0.2171	0.16
d) Trailer4_0.1CR	0	0	0.0818	0.01101	0.0712	0.0818	0.12
Trailer4_0.1CR	5	30	0.1000	0.01223	0.0877	0.1000	0.12
e) i. Trailer4_0.1CR_Fence	0	0	0.0819	0.01219	0.0697	0.0819	0.12
i. Trailer4_0.1CR_Fence	5	30	0.0997	0.01310	0.0865	0.0997	0.12
ii. Trailer4_0_1CR_Fence+flap	0	0	0.0852	0.01184	0.0732	0.0852	0.12
ii. Trailer4_0_1CR_Fence+flap	5	30	0.0877	0.01409	0.0736	0.0877	0.12
f) GEFT_Fence_at_0.01CR	0	0	0.0344	0.00916	0.0252	17.09	0.2
GEFT_Fence_at_0.01CR	2.5	0	0.0372	0.02045	0.0267	25.40	0.2
GEFT_Fence_at_0.02CR	0	0	0.0358	0.00913	0.0266	12.10	0.2
GEFT_Fence_at_0.02CR	2.5	0	0.0403	0.01065	0.0296	18.91	0.2
g) Wheeled_GEFT_Fence0.01CR	0	0	0.0558	0.00777	0.0484	11.81	0.2
Wheeled_GEFT_Fence0.01CR	2.5	0	0.0554	0.00902	0.0465	18.62	0.2
No_axle_wheeled_GEFT	0	0	0.0537	0.00795	0.0464	13.65	0.2
No_axle_wheeled_GEFT	2.5	0	0.0541	0.00909	0.0450	19.43	0.2

All the data of Table 4 assume a contiguous connection from the cabin to the box of the truck with total drag as primary interest and exhibiting the following trends:

- An initial ~30% reduction in drag through use of a full deflector configuration with the cabin; this is primarily due to the resulting induced thrust on the frontal surface which replaces some of the induced drag on the frontal surface.
- Minimal further reduction, or increase, with simple addition of a trailing taper; this is due to interference of the underbody with the taper's mechanism to reduce drag.
- An additional ~20% improvement (~50 total, "d") with a flat underbody; this is due to eliminating the destructive interference of the underbody features.
- Minimal further reduction with the simple addition of a trailing taper; this is due to a combination of the failure to further increase the induced thrust on the frontal surface and a failure to approach an effective near-free-stream pressure on the trailing taper. These failures are a result of a failure of the joining of the leading-and trailing stagnation points toward a continuous stagnation region under the underbody with higher pressure.
- An additional improvement with addition of a trailing flap of greater clearance than the fences but enough to create and extend the stagnation point throughout the underbody.

The surface profiles of Figure 13 identify that the wheels cause some destructive interference in the underbody, both within the box truck designs as well as under the modified GEFT design. Thinner wheels may reduce this destructive interference, but axels appear to have notable impact on the lower surface pressure profiles. Despite causing destructive interference, the impact of the underbody structures are much less with a flap because the velocities impacting the underbody structures are lower. As the stagnation point extends throughout the cavity, the lower velocities in the cavity reduce viscous losses and impact of the underbody obstacles is reduced. As a result, both drag and rolling losses are reduced due to the pressure expansion from the trailing edge stagnation point.

In the limit of better streamlining, the box car will approach the 3D performances of GEFT with values of L/D exceeding 20. Initial GEFT modified designs exhibit L/D near 20 without final optimization. Design towards reasonable L/D box trucks may be approached either through modifying a box truck base design or morphing GEFT prototypes to meet the criterion of box truck transports. The advantages of this further improvement are addressed in the Discussion.

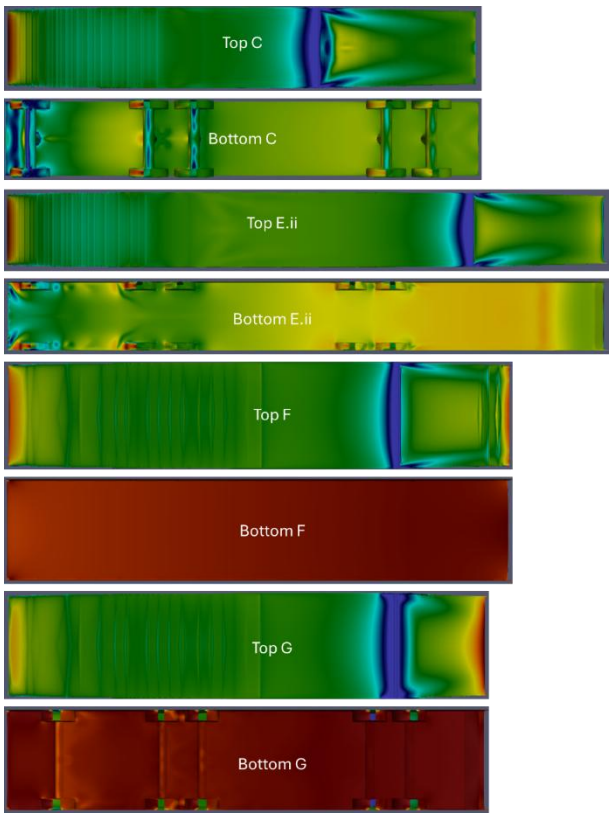

Figure 13. Upper and lower surface pressure profiles for select data of Figure 12: (c) box truck with taper, (e) ii with trailing flap, (f) representative GEFT, and (g) wheeled GEFT.

5. Discussion

A comparison of the free flight profiles of Figure 7 to the ground-effect profiles of Figure 6 identifies that the formation of higher L/D correlates with the formation of both leading-edge and trailing edge stagnation points. However, the best performance was only achieved when the propulsor discharge did not exhibit boundary-layer separation from the trailing taper which was achieved for the 25° taper of the Figure 6 airfoil but was not attained for the Figure 8b airfoil at a 45° taper per the velocity profiles of Figure 9.

The trailing taper of Lift Span Tech serves two important purposes: 1) to truncate chord length and enable higher cabin heights in a lifting body fuselage without unreasonably long chord length for beneficial [thickness]:[chord] ratios for passenger transit and 2) enabling a surface-propulsor configuration that both creates an average near-free-stream pressure on the trailing taper and near-zero velocity gradients between free streams aft the trailing taper. Preliminary results indicate these objectives can be achieved at a trailing taper pitch of 25°.

The flow vectors with downward components through the propulsor can be used to reduce the impact of boundary layer separation at higher pitch angles of trailing tapers.

5.1 Bridging of Aerial and Ground Transit

Ground-effect flight begins to bridge the gap between aerial and ground transit. Any aspects of the box truck example apply to bus and rail transit. The extension to rail creates a proven comfort with ground-transit speeds in excess of 200 mph. The result is the substantial bridging of ground an aerial transit into a continuous optimization space where box trucks have lower entry costs. Box trucks have mandates in many U.S. states for conversion to electric versus internal combustion.

The following discussion has an emphasis on box trucks because of the many aspects that apply to aerial transit and because of the position of trucking to provide the first major impacts of this technology.

5.2 Critical Trailing Stagnation Regions Properties

Formation of a trailing stagnation region between the trailing edge and the ground is critical to achieve reductions in drag beyond that from forward-section induced thrust. When properly configured, the leading-edge and trailing-edge stagnation regions join to form a region of higher pressure under the lower surface. The following are important to form this lower-surface region of higher pressure:

- Fences of low, essentially constant, clearance from leading to trailing edge.
- Formation of the trailing-edge stagnation point at and below the trailing edge.

Impacting air creates the trailing-section stagnation region; this may be air flow from the trailing taper impacting the ground or air flow from the trailing taper impacting air-flow from streamlined velocity from the lower surface.

Underbody obstacles interfere with the formation of reasonably-high-air-flow streamlined velocity along the lower surface, leading to two core options: place a lower-surface plate below any underbody obstacles to streamline flow or use a trailing flap to reduce flow through the underbody and mitigate any gradients caused by higher-velocity flows.

A third option is possible. A spoiler behind the trailing edge of the underbody may be positioned so flow along

the trailing taper impacts the forward surface of the spoiler with the resulting stagnation region extending forward. To achieve higher efficiencies, the spoiler would need to be configured to form higher pressures on forward and trailing surfaces which substantially nullify formation of induced drag from the spoiler.

The data indicate that a trailing stagnation point can replace a trailing taper to create a robust lower-surface pressure profile. The trailing stagnation point is a result of an air flow with a downward vector along trailing surface intersecting with air flow having a mostly horizontal vector flowing below the lower surface. The strongest stagnation point is a result of a flat trailing taper.

5.3 Propulsor

Figure 14 illustrates the airfoils with propulsors. Figure 6 is a variation of the 14a airfoil with a greater thickness ratio (i.e. [height]:[chord]). CFD simulation specifies air flow in x (horizontal) and y (vertical) coordinates independent of the geometry of the propulsor. For the airfoils of Figs 6 and 7, the air flow was specified as horizontal where the divergence of the flow vector from the trailing taper created a lower pressure and turned the streamlines to mostly parallel with the surface in a manner leading to good performance. For the Figure 9a-9e airfoils (i.e., 14b airfoil) good performance was only achieved with flow consisting of a downward vector component through the propulsor. The results of this paper are primarily proof of concept rather than optimization.

Stagnation regions are steady-state (or pseudo-steady-state) phenomena. The air is not stagnant; rather, the relative dynamic pressure of travelling air continuously generates pressure while the expansion of air leaving decreases pressure.

Figure 14. STL images of airfoils with propulsor "cell zones" in red, where: a) 25° taper, 10.55 cm height, 100.1 cm chord, and 5 cm X 0.5 cm propulsor and b) 45° taper, 10.4 cm height, 85.9 cm chord, and 5 cm X 0.5 cm propulsor at a -45° pitch.

5.4 Box Truck

Simulation of a cubical box has essentially pure induced drag on forward and aft surfaces, leading to high drag coefficients. Adding an upper surface curvature to the frontal section allows diverging flow from the forward stagnation point to create induced thrust and reduce the drag.

Addition of a trailing taper can reduce the magnitude of the induced thrust on the aft surface. With the trailing taper, boundary layer separation still occurred and was only alleviated with a propulsor. At an optimal configuration the propulsor can eliminate boundary layer separation and create an average pressure on the taper near free-stream pressure. An average pressure near free stream pressure approaches performance with neither net induced drag nor net induced thrust on the trailing taper.

With further refinement of the box truck toward the GEFT design, drag is reduced on the undercarriage and aerodynamic lift is generated. Since pressure extends over a surface at the speed of sound, a streamlined lower surface impacts air flow throughout the airfoil surface. For a GEFT-type box truck airfoil, the ability to replace wheel-suspension with aerodynamic suspension can be achieved with hovercraft or air flow dynamics where the air flow dynamics are much more energy-efficient. At higher velocities (e.g., 85 mph) lifts can be generated to substantially nullify wheel friction losses of the trailer where a lead tractor would maintain some wheel traction to provide conventional guidance over highways.

Devices such as side skirts, boat tails, and roof air deflectors are able to reduce drag. These devices have two shortcomings: a) the devices can reduce extreme drag losses by eliminating some boundary layer separation but lower pressures on aft surfaces still create induced drag and b) the devices have limited capabilities to address undercarriage drag features such as wheels [56].

Table 5 summarizes the lost work for steady-level transit of an example tractor-trailer box truck. For 61 kW of aerodynamic resistance there is 44 kW of rolling resistance. GEM designs can substantially eliminate the 44 kW of loss while further reducing the aerodynamic resistance.

For an optimized GEFT design, the pressure drag can approach zero; however, there are diminishing returns for taking pressure drag to levels much less than viscous drag. Most of the drag and rolling resistance can be eliminated when applying GEFT technology to roadway vehicles. Further reductions in lost work can be attained when using regenerative braking.

Values of air's relative dynamic pressure are summarized in Table 6. At low fence clearances, GEFT are able to

approach air's dynamic pressure in the cavity. Without any lift from upper surfaces, this translates to a lift coefficient of 1.0. When allowing for a lift coefficient of 1.2; loads of one ton per ten feet of bed are attainable. The impact of aerodynamic suspension can be significant for many vehicles, especially in applications with travel containing empty or reduced loads.

Table 5. Example lost work for steady-level transit for a tactor-trailer box truck [57, 58].

	Power (kW)		(%)
Fuel Input	343		
Engine Losses	193		
Idling Fuel Use	3.6		
Accessory Loads	15		
Drivetrain Losses	10		
Aerodynamic Losses	61		
Trailer Tail		3.39	31%
Trailer Underbody		4.07	38%
Trailer Gap		1.36	13%
Tractor Aero Details		2.03	19%
Rolling Resistance	44		
Inertia/Braking Losses	15		

Table 6. Air's dynamic pressure at density of 1.25 kg/m^3 and trailer width of 8.5 ft.

U (m/s)	U mph	Pa kg/m/s2	Load lb/ft
30	67	563	100
40	90	1000	178
50	112	1563	277

Many box truck applications would benefit from GEFT embodiments which include Lift Span Tech. For trailers in general, solar power and regenerative braking enable power-assist modes of operation that can increase efficiency and reduce the demands on the vehicle towing the trailer. Open trailers can benefit from lower-cavity configurations; this data identifies that open trailers should have frontal deflectors, trailing taper, and tarps to assist in the formation of robust pressure profiles in lower cavities.

Additional data as well as best practices will develop with applications of this technology. At least to some extent, the expectation is that trailers could be extended as necessary to increase aerodynamic lift and improve net present values. This would include extendable/retractable configurations.

Table 7. Summary of reduced energy consumption due to reduced aerodynamic drag and reduced wheel suspension for steady-state driving.

	Lost Work	70% Drag Reduction + 70% Regenerative Braking		50% Reduction in Wheel Suspension		Total
	kW	Saved (kW)		Saved (kW)		
Idling Fuel Use	3.6	--		--		
Accessory Loads	15	--		--		
Drivetrain Losses (drag)	*5.8*	4.1	2.7%	--		2.7%
Drivetrain Losses (rolling)	*4.2*	--		2.1	1.4%	1.4%
Aerodynamic Losses	61	42.7	28.7%	--		28.7%
Rolling Resistance	44	--		22	14.8%	14.8%
Inertia/Braking Losses	15	10.5	7.1%	--		7.1%
TOTAL	**148.6**	**53.2**	**35.8%**	**22.0**	**14.8%**	**50.6%**

5.5 L/D Efficiency Enhancement

The addition of L/D efficiency enhancements to the previously-discussed drag reduction enhancements can address wheel resistance losses of Table 5. Whereas a 70% reduction in drag losses can result in a 34% reduction in energy consumption for a box truck at steady-level driving, a 70% reduction in drag plus a 50% reduction is suspension can result in a 51% reduction in energy at steady-level driving.

The fraction of total suspension provided by aerodynamic lift is a degree of freedom in box truck operation, where at optimal design the factors that impact this fraction are

steady-level travel velocity and load density (kg/m^2). At least some wheel suspension is needed to maintain control with conventional steering and traction; however, an 80% reduction on load is plausible. Data suggest that an 80% reduction in drag is also possible. At 80% reduction in both drag and wheel suspension, a 66% reduction in energy consumption is possible.

5.6 Regenerative Braking

Regenerative braking can recover 70% to 80% of the inertial/braking loss. This increases the 66% to a 68%. Perhaps of greater impact is that the regenerative braking can be a trailer component versus a cab component.

Air-based propulsion on a box trailer is a part of the broader topic of trailer-assisted propulsion. A barrier to trailer-assisted propulsion is the cost of the power and energy sources of a trailer. Regenerative braking is a reasonable source of energy for trailer-assist propulsion since it would not require refueling or significant maintenance.

An additional source of low-maintenance clean power and energy for a trailer is a solar-power canopy.

5.7 Solar Power Canopies

In contemporary configurations, the amount of solar energy that can be collected on a truck is too low to have a significant impact. However, as the cost of solar power decreases, the cost of canopies with solar cells becomes increasingly negligible when mass produced by printing and laminating methods as a structural body material. The additional leveraging of direct solar power as illustrated by Figure 2 further improves the economics when using lift Span technology.

In the absence of the solar power, solar power mass produced at less than $0.01 / kWh can replace fuel at $0.18 / KWh as based on annualized costs inclusive of capital costs [59]. When capitalizing on the leveraging of thrust as illustrated by Figure 2,the economics further improve as well as with considerations for reduction in drivetrain costs, engine costs, and maintenance related to rolling/mechanical resistance. The direct use of solar power to replace fuel has a huge upside potential, and this application can provide the demand for solar panels to make that happen. By placing solar panels on vehicles, the demand on grid power is not an issue and can be resolved if parked vehicles provide power to the grid. Broader issues also emerge on this subject such as pending mandates in states to use electric trucks where increased vehicular efficiencies reduce the battery costs and weights for these trucks.

When supplemented with battery storage and regenerative braking, logistics of operation function for both trailer-assisted propulsion embodiments built within both the tractor and the trailer. The benefits apply to the broader sectors of trailers and buses with structures similar to box trucks. For delivery vehicles, extended parking time and regenerative braking could lead to full displacement of liquid fuels.

5.8 Benchmark Numbers for Large Semitrucks

The heavy loads of semitrucks are at odds with use of solar power. Table 8 summarizes reported values and solar energy conversions used to estimate the meters of panel length needed to collect the energy needed for a semi box truck. Table 8 summarizes the lengths for comparison to a standard semi box truck length of 80 ft.

Table 8. Solar energy conversions for Table 9 estimates of trailer lengths. *Values extended to Table 9.

Value	Formula
137000 BTU/gallon	Commonly reported chemical energy diesel
5 gallons/hour	Based on 60 mph and 10 mpg for semi boxtruck
241,000 W	Conversion of 3.4 Btu/hr = 1 W
175 W/m^2	Power produced by a photovoltaic cell (moderately sunny location)
226 m*	241,000 (W) / 174 (W/m^2) / 2.45 (m wide trailer) x 60% (diesel eng. Eff.)
149 m	34% reduction in energy per Table 7 (from drag reduction)
111 m	51% reduction in energy per Table 7 (from drag and wheel friction reduction) 111 m = 226 m x 49%

For a load basis, the following factors provide a base truck case: 35,000 lb empty, 80,000 lb loaded. Applying 0.5 tons/10 ft of aerodynamic lift at 60 mph per Table 6, the 80,000 lb are distributed from 1100 lb/ft for 727 ft to achieve full solar suspension. Table 9 summarizes the base case required length for different use scenarios based on load. The "Load Basis" summary of Table 9 primarily identifies if aerodynamic lift a 60 mph is adequate to achieve the 50% reduction in rolling resistance of Table 7, with the result that half the semitruck lift can be attained for many applications, including full lift for empty or near-empty box trailers. In many instances aerodynamic lift

can be used to reduce rolling losses to the minimum needed to use wheels to navigate roadways.

Table 9. Case study length numbers for box truck. Solar energy analysis identifies if the surface area is sufficient to provide the needed power. Load data evaluates the extent to which aerodynamic lift can replace wheel suspension toward reduced rolling losses. *See Table 8.

	Solar Energy Basis		Load Basis	
	ft	m	ft	m
Base Case	741	226*	72 7	22 1.7
Reduced Drag/Friction & fuel conversion efficiency	364	111*		
PV on sides (doubling power)	182	55.5		
Half Load, Half Lift			18 2	55. 4
Half Load, Half Lift, 90 mph			92	27. 7
Light Packages, Light Design			< 90	27. 7
Empty			< 90	27. 7
Passenger Bus			< 90	27. 7

The limiting factor is the ability to place enough solar panels on a truck to provide the propulsion for the Table 7 use scenarios. The best-case scenario is for solar power is to provide about half the energy needs (91 ft semitruck versus 182 ft needed to provide the solar power). The following factors will lead to more than 50% of energy provided by direct solar on trucks:

- 50% or greater aerodynamic suspension.
- 70% or greater reduction in drag.
- Reduced accessory and idling loads, which were not included since they compensate for electric motor efficiency.
- Increasing photovoltaic (PV) cell power density beyond 175 W/m^2; which can be achieved with improved PV efficiency and sunnier locations.

The vehicle configurations of this study were not optimized. Therefore, it is possible that 100% of energy can be provided by solar power through advances on multiple of these factors.

Reduced drag and rolling resistances of Table 7 provide a 51% reduction in energy requirements with over 50% solar power; the result is a 75% to 100% reduction in fuel for daylight transit. These reductions are substantially enabling for batteries or fuel cells to displace fossil fuels in application.

A limiting factor on solar is lack of availability at night and lack of reliability due to weather. The advantages include using direct solar power costing about 1 cent/kWh (annualized cost) to displace diesel costing about 18 cent/kWh and using solar power when parked to charge batteries or provide power to the electrical grid. The economics appear to be beneficial even trucks with requiring batteries or fuel cells to supplement the solar power.

For many routes, box trucks are empty for return trips, but fuel consumption of conventional empty box trucks is >80% of the full load; for empty or light trucks a <90 ft option emerges where aerodynamic lift can be used to full capacity to reduce energy consumption while maintaining sufficient wheel friction to drive on highways.

For buses, the specific loads (kg/m^2) can be low enough to maximize aerodynamic lift and provide high efficiency. This would provide passenger space similar to the best first-class airliner service including reasonable sleeping and entertainment options.

5.9 Aerial Transit versus Roadway Transit

Lift Span Tech can be used to improve efficiency of both aircraft and box trucks. More specifically, GEM bridges the gap between air and ground transit including the topics of air taxis and autonomous vehicles. Existing highways, railways, subways, and waterways may serve as transit corridors for new generation GEM that are able to effectively use these corridors with use of free flight to transition between corridors where benefits of reduced distance or traffic congestion compensate for the lower efficiency of free flight versus ground-effect flight.

Significant energy savings during steady-level flight and increased aerodynamic suspension at higher velocities provide additional incentives to provide un-interrupted high-speed transit on highways. This is possible on interstates and express lanes with significant implications on passenger transit. In societal transition of transit, an initial phase of platoons of vehicles traveling at 90 mph and full solar power would replace much of the rail transit. When rail transit is sufficiently low, rail corridors would be transformed into high-speed corridors with travel velocities up to and in excess of 300 mph.

For these ground-based systems, there are energy benefits to keeping specific weight (kg/m^2) lower, which translates to: i) increased levels of comfort for travel, ii) red-eye

service with comfort for sleeping, and iii) improved performance business or entertainment during transit. The result is reduced total transit times and low-cost transit that displaces hotel costs. The implications are far-reaching.

5.10 Lift Span Tech

In addition to the advantages cited in the Background section, the following advantages have been identified for Lift Span Tech:

- A steeper pitch after the propulsor can, under the right conditions, lead to a higher impact of flow with the ground and lead to higher pressure as a trailing edge stagnation point extending from the ground to the lower surface of the vehicle.
- Both increased lift and L/D efficiency depend on the higher pressures of the trailing-edge stagnation region extending through the vehicle's lower cavity which is easier to achieve with the truncated length made possible with the steeper trailing taper.
- By generating aerodynamic lift per higher pressures throughout the underbody, Lift Span Tech is able to reduce mechanic friction (i.e. rolling losses) which is a major advance since there are few solutions to the mechanical resistance issue.

Lift Span Tech has applications in free flight aircraft and ground-effect aircraft. The background cites other work identifying how Lift Span Tech is able to overcome induced drag, and because induced drag is an issue with essentially all ground vehicles, the box truck provides a good case study to identify broader implications. Those broader implications were identified, including the rare systematic solution to reducing mechanical resistance (e.g. rolling losses). One of the best contemporary solutions to mechanical resistance is steel-on-rail transit (i.e., trains); this technology has the potential to provide substantial increase in transit efficiency versus trains.

Conclusions

Boundary layer separation is commonly encountered when a change in pitch angle exceeds a threshold value where laminar airflow along the surface may not be contained. This indicates that small perturbations in the air flow could restrain the onset of boundary layer separation. The data of this paper demonstrates that propulsors are able to provide this small perturbation with resulting high [gain in L/D efficiency]:[loss in effective thrust]. Lift Span Tech is able to further reduce lost work by reducing the induced drag that remains when boundary-layer separation is eliminated.

However, Lift Span Tech has limited ability to reduce drag due to wheels on underbodies and rolling resistance. Ground-effect flight is able to eliminate most of these remaining underbody and wheel resistance losses. For a towed-platform configuration, a tractor that retains some wheel traction can provide guidance while the primarily load as supported by the trailer could benefit from highly-efficient ground effect suspension.

Two substantial reductions in drag for box trucks are possible:

1. The first is when a leading-edge stagnation region forms when the leading edge is in the proximity of the lower surface causing oncoming air to flow upward and create induced thrust at the front section of the vehicle.
2. The second is when a trailing-edge stagnation region forms and extends forward to a leading-edge stagnation region creating higher pressures, and a continuous lower surface stagnation region, along the entire lower surface. This occurs under two circumstances: a) horizontal streamlined air along a substantially obstacle-free lower surface impacts streamlined air flowing along a trailing taper and b) streamlined air flowing along a trailing taper impacts the ground creating a high pressure where a trailing flap has a trailing edge low enough to the ground for the trailing edge to be engulfed by the trailing-edge stagnation region. The latter circumstance has two important characteristics: i) air's velocity through the lower cavity reduced to the point where pressure gradients caused by obstacles in the underbody are inconsequential and ii) higher pressures on leading and trailing surfaces of the flap substantially cancel.

When both reductions are achieved, it is possible to form aerodynamic lift on the lower surface of a vehicle and trailer to support over a ton of lift per ten feet of length which reduces wheel friction losses to complement reductions in aerodynamic drag. With additional benefits of reducing wheeled suspension combined with regenerative braking, a synergy for transit technologies emerges. Electric trucking and bus service is not only viable, but emerges offering significant savings in energy with advanced applications offering reductions in transit time for many routes. If a coordinated evolution of transit were put in place, rail transit could emerge using existing

railway tracks for transit systematically in excess of 200 mph and often in excess of 300 mph.

Enabled with substantial improvements in efficiency and substantial box car surface areas, solar power is positioned to further reduce transit costs with a sustainable and environmentally-friendly energy source. The benefits of this approach apply to applications ranging from aircraft to box trucks. Applications traverse the gamut of transportation sector including autonomous drone and air taxi applications. A next step is to set in motion commercial efforts on implementing this technology to meet imminent mandates on electric trucks.

Abbreviations

2D	two dimensional.
3D	three Dimensional
AR	aspect ratio, defined as the span divided by a representative longitudinal chord length
Camber	curvature of an airfoil characterized as a deviation from straight as either a fraction of the chord length or percent of a chord length (e.g., 0.01 c or 1%)
C_d	drag coefficient
CFD	computational fluid dynamics
c, Chord	chord, distance from leading edge to trailing edge of an airfoil or wing
C_l	lift coefficient
Curl	a favorable flow of air from below the leading edge to the upper surface resulting in a low-pressure area on the upper surface immediately behind the leading edge.
D	drag, form drag is due to pressure on the surface, total drag as equal to sum of form and shear drag
GEM	Ground Effect Machine
L/D	lift-drag ratio, the primary measure of airframe efficiency
	lift pressures = pressures that generate aerodynamic lift such as lower pressures on upper surfaces and higher pressures on lower surfaces.
Loss	lost energy term of Bernoulli equation (J/kg)
P	pressure (N/m^2) pressure is absolute pressure unless a subscript of G identifies gauge pressure with reference as free stream pressure, 1 atm
Source	a Source of propulsion, a Source generates thrust
u	velocity of air relative to an airframe
t/c	thickness to chord ratio, thickness is a maximum vertical dimension
VTOL	vertical takeoff and landing
α_P	angle from horizontal (°), subscript P identifies angle of a point on a line or surface
ρ	density (kg/m^3), typically density of air

Conflict of interest

The authors declare no conflicts of interest regarding the current research.

Author Contribution

Galen Suppes proposed the research problem, designed experiments, and performed majority of writing.

Adam Suppes performed computational fluid dynamics and reduced simulation results to figures and tables in good format.

Harith H. Al-Moameri verified the analytical methods.

References

[1] Abbas, Z., Mansoor, M., Habib, M., and Mehmood, Z., "Review: MEMS sensors for flow separation detection," *Microsystem Technologies*, Vol. 29, No. 9, 2023, pp. 1253–1280. 10.1007/s00542-023-05513-x

[2] Simpson, R.L., "untitled," *Ann. Rev. Fluid Mech.*, Vol. 21, 1989, pp. 205–34.

[3] Veerasamy, D., Atkin, C.J., and Ponnusami, S.A., "Aerofoil wake-induced transition characteristics on a flat-plate boundary layer," *Journal of Fluid Mechanics*, Vol. 920, 2021, pp. A29. 10.1017/jfm.2021.452

[4] Cotte, B., Roy, S., Raus, D., and Oueini, R., "Towards a semi-empirical trailing edge noise model valid for attached and separated turbulent boundary layers," *28th AIAA/CEAS Aeroacoustics 2022 Conference*, 2022, https://doi.org/10.2514/6.2022-3103

[5] Rodriguez, I., Lehmkuhl, O., and Borrell, R., "Effects of the Actuation on the Boundary Layer of an Airfoil

at Reynolds Number Re = 60000," *Flow, Turbulence and Combustion*, Vol. 105, No. 2, 2020, pp. 607–626. 10.1007/s10494-020-00160-y

[6] Kumar, K., Kumar, P., and Singh, S.K., "PASSIVE CONTROL OF BOUNDARY LAYER SEPARATION USING SINGLE AND MULTIPLE SLATS ON THE AIRFOIL," *International Journal of Fluid Mechanics Research*, Vol. 48, No. 2, 2021, 10.1615/InterJFluidMechRes.2021033106

[7] Jarmon, C.M., Lang, A.W., and Hubner, J., "Wind Tunnel Investigations of Sharkskin Inspired Passive Flow Control Devices," *AIAA SciTech 2024 Forum*, 2024, https://doi.org/10.2514/6.2024-1938

[8] Cross, A., "Experimental Investigations into Shark Skin Inspired Active Flow Control Mechanisms," 2022, https://www.proquest.com/openview/9e436ff604c8239aed2a2df17af8ca27/1?pq-origsite=gscholar&cbl=18750&diss=y

[9] Huang, W., Wu, H., Yang, Y., Yan, L., and Li, S., "Recent advances in the shock wave/boundary layer interaction and its control in internal and external flows," *Acta Astronautica*, Vol. 174, 2020, pp. 103–122. 10.1016/j.actaastro.2020.05.001

[10] Atik, H., Kim, C.-., Dommelen, L.L.V., and Walker, J.D.A., "Boundary-layer separation control on a thin airfoil using local suction," *Journal of Fluid Mechanics*, Vol. 535, 2005, pp. 415–443. 10.1017/S002211200500501X

[11] Wang, A., and Lai, H., "Control of separated flow at low Reynolds number around NACA0012 airfoil by boundary layer suction," *Journal of Physics: Conference Series*, Vol. 2707, 2024, pp. 012122. 10.1088/1742-6596/2707/1/012122

[12] Mirhashemi, A., Chapman, J.W., Miller, C.J., "Tail-mounted engine Architecture and Design for the Subsonic Single Aft Engine Electrofan Aircraft," San Diego, CA,

[13] Jansen, R.H., Kiris, C.C., Chau, T., "Subsonic Single Aft Engine (SUSAN) Transport Aircraft Concept and Trade Space Exploration," San Diego, California,

[14] Russo, O., and Aprovitola A, de Rosa D, Pezzella G, Viviani A., "Computational Fluid Dynamics analyses of a wing with distributed electric propulsion," *Aerospace*, Vol. 10, No. 1, 2022, https://doi.org/10.3390/aerospace10010064

[15] Serrano, J., Tiseira, A., García-Cuevas, L., and Varela, P., "Computational Study of the Propeller Position Effects in Wing-Mounted, Distributed Electric Propulsion with Boundary Layer Ingestion in a 25 kg Remotely Piloted Aircraft," *Drones*, Vol. 5, 2021, pp. 56. 10.3390/drones5030056

[16] Gohardani, A., Doulgeris, G., and Singh, R., "Challenges of future aircraft propulsion: A review of distributed propulsion technology and its potential application for the all electric commercial aircraft," *Progress in Aerospace Sciences*, Vol. 47, 2011, pp. 369–391. 10.1016/j.paerosci.2010.09.001

[17] Pascual, B. R., Vos, R., "The Effect of Engine Location on the Aerodynamic Efficiency of a Flying-V Aircraft | AIAA SciTech Forum," 2020, https://arc.aiaa.org/doi/10.2514/6.2020-1954

[18] Snyder, M.H., Zumwalt, G.W., "Effects of wingtip-mounted propellers on wing lift and induced drag. | Journal of Aircraft," *J. Aircraft*, Vol. 6, No. 5, 1969, pp. 392–397.

[19] Erhard, R., Clarke, M., and Alonso, J., "A Low-Cost Aero-Propulsive Analysis of Distributed Electric Propulsion Aircraft," January 11, 2021, 10.2514/6.2021-1200

[20] Cunningham, M., Nigam, N., Ayyalasomayajula, S., "Integrated Vehicle-Propulsion-Control Design Architecture for Distributed Electric Propulsion-Enabled Aircraft," 2022-06-27, 10.2514/6.2022-3484

[21] Loth, J., Loth, F., "Induced drag reduction with wing tip mounted propellers | Fluid Dynamics and Co-located Conferences," *AIAA 2nd Applied Aerodynamics Conference*, August, 1984, pp. 1–8.

[22] Sinnige, T., van Arnhem, N., Stokkermans, T. C. A., Eitelberg, G., Veldhuis, L.M., "Wingtip-Mounted Propellers: Aerodynamic Analysis of Interaction Effects and Comparison with Conventional Layout | Journal of Aircraft," *J. Aircraft*, Vol. 56, No. 1, 2019, pp. 295–312.

[23] Cole, J., Krebs, T., Barcelos, D., and Bramesfeld, G., "Influence of Propeller Location, Diameter, and Rotation Direction on Aerodynamic Efficiency," *Journal of Aircraft*, Vol. 58, 2020, pp. 1–9. 10.2514/1.C035917

[24] Krishna, Y.C., and Venkatesh, T.N., "Numerical investigation of aerodynamically efficient wing tip-mounted propeller configuration using coupled

RANS–BEM approach," *Aircraft Engineering and Aerospace Technology*, Vol. 95, 2023, 10.1108/AEAT-09-2022-0254

[25] Kim, H.D., Perry, A.T., and Ansell, P.J., "A Review of Distributed Electric Propulsion Concepts for Air Vehicle Technology," *2018 AIAA/IEEE Electric Aircraft Technologies Symposium (EATS)*, 2018, pp. 1–21. 10.2514/6.2018-4998

[26] Zhang, X, Zhang, W., Li, W., Zhang, X., Lei, T., "Experimental research on aero-propulsion coupling characteristics of a distributed electric propulsion aircraft - ScienceDirect," *Chinese Journal of Aeronautics*, Vol. 36, No. 2, 2023, pp. 201–212.

[27] Suppes, A., and Suppes, G., "Thermodynamic Analysis of Distributed Propulsion," *Research Square*, 2023, pp. 1–26. 10.21203/rs.3.rs-4670270/v1

[28] Suppes, G., and Suppes, A., "Critical Data and Thinking in Ground Effect Vehicle Design," Cambridge University Press, Cambridge Open Engage, 2024. https://www.cambridge.org/engage/https://doi.org/10.33774/coe-2024-76mzx

[29] Bulat, P., Chernyshov, P., Prodan, N., and Volkov, K., "Control of Aerodynamic Characteristics of Thick Airfoils at Low Reynolds Numbers Using Methods of Boundary Layer Control," *Fluids*, Vol. 9, No. 1, 2024, pp. 26. 10.3390/fluids9010026

[30] Deviparameswari, K., Meenakshi, S., Akshay Kumar, N., Vigneshwaran, R., Rohini Janaki, B., Vinsiya Maria, A., Keerthana, N., Surya, B., Vetrivel, M., Thianesh, U.K., Rajarajan, S., Manikandan, P., "The Effects of Ground Clearance and Boundary Layer Blockage Factor on the Aerodynamics Performance of the Hyperloop Pod and Transonic Ground-Effect Aircraft | AIAA AVIATION Forum," *AIAA Aviation Forum*, 2021, https://doi.org/10.2514/6.2021-2586

[31] Qu, Q., Wang, W., Liu, P., and Agarwal, R.K., "Airfoil Aerodynamics in Ground Effect for Wide Range of Angles of Attack," *AIAA Journal*, Vol. 53, No. 4, 2015, https://doi.org/10.2514/1.J053366

[32] Qu, Q., Zuo, P., Wang, W., Liu, P., and Agarwal, R.K., "Numerical Investigation of the Aerodynamics of an Airfoil in Mutational Ground Effect," *AIAA Jouranl*, Vol. 53, 2015, https://doi.org/10.2514/1.J054155

[33] Lee, S., and Lee, J., "Aerodynamic analysis and multi-objective optimization of wings in ground effect," *Ocean Engineering*, Vol. 68, 2013, pp. 1–13. https://doi.org/10.1016/j.oceaneng.2013.04.018

[34] Lee, S., and Lee, J., "Optimization of Three-Dimensional Wings in Ground Effect Using Multiobjective Genetic Algorithm," *Journal of Aircraft*, Vol. 48, No. 5, 2012, https://doi.org/10.2514/1.C031328

[35] Lee, J., "Computational analysis of static height stability and aerodynamics of vehicles with a fuselage, wing and tail in ground effect - ScienceDirect," *Ocean Engineering*, Vol. 168, 2018, pp. 12–22. https://doi.org/10.1016/j.oceaneng.2018.08.051

[36] Hu, H., Zhang, G., Li, D., Zhang, Z., Sun, T., and Zong, Z., "Shape optimization of airfoil in ground effect based on free-form deformation utilizing sensitivity analysis and surrogate model of artificial neural network - ScienceDirect," *Ocean Engineering*, Vol. 257, 2022, pp. 111514. https://doi.org/10.1016/j.oceaneng.2022.111514

[37] Halloran, M., and O'Meara, S., "Wing in Ground Effect Craft Review," Aeronautical and Maritime Research Laboratory, Melbourne Victoria 3001 Australia, 1999. https://apps.dtic.mil/sti/pdfs/ADA361836.pdf

[38] Anonymous "Ground effect machine," Vol. 7953/71, No. GB1347352, 1974, https://patents.google.com/patent/GB1347352A/en?oq=London+1347352

[39] Suppes, A., Suppes, G., Lubguban, A., and Al-Maomeri, H., "An Airfoil Science Including Causality," *Cambridge Engage*, 2024, 10.33774/coe-2024-w4qtp

[40] Suppes, A., Suppes, G., Lubguban, A.A., and Al-Moameri, H.H., "Kinetic theory of gases: explanation of aerodynamic lift," *Aviation (in Review)*, 2024,

[41] Suppes, G., and Suppes, A., "Ground Effect Flight Transit (GEFT) – Approaches to Design," Cambridge University Press, Cambridge Open Engage, 2024. https://www.cambridge.org/engage/coe/article-details/66b2340b01103d79c5e7ab2310.33774/coe-2024-2c87q

[42] Suppes, A., and Suppes, G., "Ground Effect Flight Transit (GEFT) – Towards Trans-Modal

Sustainability," Vol. 1, 2024, https://doi.org/10.33774/coe-2024-prxvr

[43] Suppes, G., and Suppes, A., "Ground Effect Flight Transit (GEFT) in Subways," Vol. 1, 2024, https://doi.org/10.33774/coe-2024-6w0lw

[44] Suppes, A., and Suppes, G., "New Benchmarks in Ground-Effect Flight Energy Efficiency," July 102024https://www.researchsquare.com/article/rs-4707178/v1https://doi.org/10.21203/rs.3.rs-4707178/v1 [cited Jul 29 2024].

[45] Suppes, A., and Suppes, G., "Aerodynamic Lift Railcar Suspension – Faster, Quieter, More-Efficient," *Railway Engineering Science*, Submitted for Review, pp. 1–16.

[46] Suppes, A., and Suppes, G., "Poster: Highly-Efficient low-AR aerial vehicles in urban transit (available at http://www.terretrans.com/opensource.html)," *Transportation Research Board 104rd Annual Meeting*, January 7, 2024,

[47] Suppes, A., and Suppes, G., "Highly-Efficient Low-AR aerial vehicles in urban transit," *Proceedings of the 2014 Transportation Research Board Annual Meeting*, January, 2024,

[48] Suppes, G., and Suppes, A., "Understanding Thin Cambered Airfoils and their Solar Aircraft Applications," *Research Square*, 2023, pp. 1–29. https://doi.org/10.21203/rs.3.rs-4670250/v1

[49] Klose, B., Spedding, G., and Jacobs, G., "Direct numerical simulation of cambered airfoil aerodynamics at Re = 20,000," 2021, https://doi.org/10.48550/arXiv.2108.04910

[50] Michna, J., and Rogowski, K., "Numerical Study of the Effect of the Reynolds Number and the Turbulence Intensity on the Performance of the NACA 0018 Airfoil at the Low Reynolds Number Regime," *Processes*, Vol. 10, 2022, pp. 1004. 10.3390/pr10051004

[51] Lee, D., Nonomura, T., Oyama, A., and Fujii, K., "Comparison of Numerical Methods Evaluating Airfoil Aerodynamic Characteristics at Low Reynolds Number," *Journal of Aircraft*, Vol. 52, 2015, pp. 296–306. 10.2514/1.C032721

[52] Williams, O., Samuell, M., Sarwas, E.S., Robbins, M., and Ferrante, A., "Experimental Study of a CFD Validation Test Case for Turbulent Separated Flows," *AIAA Scitech 2020 FOrum*, 2020, https://doi.org/10.2514/6.2020-0092

[53] Suppes, G., and Suppes, A., "Ground Effect Vehicle," Vol. PCT/US24/35242, 2024, pp. 1–32. www.hs-drone.com

[54] Leifsson, L., Ko, A., Mason, W., Schetz, J., Haftka, R., and Grossman, B., "Multidisciplinary Design Optimization for a Blended Wing Body Transport Aircraft with Distributed Propulsion," 2011,

[55] Wu, R., Soutis, C., Zhong, S., and Filippone, A., "A morphing aerofoil with highly controllable aerodynamic performance," *The Aeronautical Journal*, Vol. 121, 2016, pp. 1–19. 10.1017/aer.2016.113

[56] National Research Council, "Review of Aerodynamic Drag Reduction Devices for Heavy Trucks and Buses," Transport Canada, Government of Canada Website, 2018. https://tc.canada.ca/en/programs/non-funding-programs/ecotechnology-vehicles-program/review-aerodynamic-drag-reduction-devices-heavy-trucks-buses

[57] Committee on Assessment of Technologies and Approaches for Reducing the Fuel Consumption of Medium- and Heavy-Duty Vehicles, Phase Two, "Reducing the Fuel Consumption and Greenhouse Gas Emissions of Medium- and Heavy-Duty Vehicles, Phase Two: First Report," The National Academies Press, 500 Fifth St. NW Washington DC, 2014, pp. 67–72.

[58] Anonymous "21st Century Truck Technical Goals," [online database]https://www.energy.gov/eere/vehicles/21st-century-truck-technical-goals [cited Dec 3 2024].

[59] Anonymous "2030 Solar Cost Targets," [online database]https://www.energy.gov/eere/solar/articles/2030-solar-cost-targets [cited Nov 26 2023].